Phonon analog of topological nodal semimetals

Hoi Chun Po, Yasaman Bahri, and Ashvin Vishwanath

Phys. Rev. B **93**, 205158 — Published 31 May 2016

DOI: 10.1103/PhysRevB.93.205158

Phonon analogue of topological nodal semimetals

Hoi Chun Po, Yasaman Bahri, and Ashvin Vishwanath[1]

[1]*Department of Physics, University of California, Berkeley, California 94720, USA*

Topological band structures in electronic systems like topological insulators and semimetals give rise to highly unusual physical properties. Analogous topological effects have also been discussed in bosonic systems, but the novel phenomena typically occur only when the system is excited by finite-frequency probes. A mapping recently proposed by Kane and Lubensky [Nat. Phys. **10**, 39 (2014)], however, establishes a closer correspondence. It relates the zero-frequency excitations of mechanical systems to topological zero modes of fermions that appear at the edges of an otherwise gapped system. Here we generalize the mapping to systems with an intrinsically gapless bulk. In particular, we construct mechanical counterparts of topological semimetals. The resulting gapless bulk modes are physically distinct from the usual acoustic Goldstone phonons, and appear even in the absence of continuous translation invariance. Moreover, the zero-frequency phonon modes feature adjustable momenta and are topologically protected as long as the lattice coordination is unchanged. Such protected soft modes with tunable wavevector may be useful in designing mechanical structures with fault-tolerant properties.

I. INTRODUCTION

Correspondences between bosonic and fermionic problems have long been an indispensable tool for both solving and understanding model systems. Other than a few known exceptions, however, conventional mappings like the Jordan-Wigner transformation and bosonization are generally exact only in one spatial dimension[1,2]. For free particles, both bosonic and fermionic Hamiltonians are characterized by the single-particle Hamiltonians. The statistics of the particles are reflected in the different algebras invoked in their canonical transformations[3]. In addition, for stable bosonic system the single-particle Hamiltonian is required to be positive semi-definite[4,5]. Despite such differences, one can nonetheless establish an equivalence between the spectra of a bosonic and a fermionic problem by factorizing the corresponding matrices[4–6]. Although this approach is limited to free or weakly interacting particles, unlike most other mappings, for certain problems it is manifestly local in any dimensions. It is therefore of interest to explore the extent to which this correspondence can provide a new perspective.

The recent realization of the existence of surface modes dictated by topological properties of the bulk has generated immense interest across the community[6–12]. Topological insulators, for instance, are electronic systems that host protected conducting surface states but are insulating in their bulk[7]. Within the free fermion description, the existence of these robust surface states can be predicted, via the bulk-boundary correspondence, by computing the topological invariants associated with the occupied Bloch bands[7]. More recently, certain mechanical (spring-mass) problems were independently found to host robust zero-energy modes localized at boundaries[13]. The boson-fermion mapping proposed by Kane and Lubensky[6] demonstrates that these phenomena are the two sides of the same coin. In particular, the mapping naturally relates the ground state properties of a phonon problem (i.e. the spectrum in the zero-frequency limit) to that of a particle-hole symmetric fermionic problem at half-filling, for which the Fermi energy is naturally pinned to zero.

In Ref. [6], the boson-fermion mapping was applied to mechanical frames with a gapped spectrum (aside from the acoustic modes), and these systems can be viewed as the phonon analogues of weak topological insulators. The topological nature of the bulk spectrum is reflected as zero-frequency modes or states of self-stressed localized at the boundaries[6] or defects[12]. A natural step forward is to identify phonon analogues of topological nodal semimetals (TNS), which feature gapless nodes in the bulk spectrum protected by nontrivial band topology, and can lead to interesting surface Fermi-arcs[14].

Previous works have demonstrated the construction of TNS analogues in bosonic systems, such as photonic crystals[15], acoustic systems[16] and even spring-mass models[17]. The associated band touchings, however, occur at non-zero frequencies and the topological features are irrelevant when one is interested in only the low energy excitation of the system.

In this work, we seek to construct phonon analogues of TNS with protected zero-energy modes in the linearized phonon spectrum. In particular, we consider pinned, periodic spring-mass models. One may expect such models, if stable and not 'floppy' (having an extensive number of zero modes), should generically have a fully gapped phonon spectrum at zero phonon frequency. Contrary to this expectation, we show that bulk node with $\omega(\boldsymbol{k}_c) = 0$ can in fact appear without fine-tuning in certain isostatic models, and their existence is rooted in the topological protection of the corresponding fermionic TNS. These systems correspond to metamaterials or mechanical structures with robust extended soft modes which can be employed as building blocks of more complex structures requiring both rigidity for stability and flexibility for functionality[11,12]. Fault tolerance, provided by topological protection, is highly desirable for applications in which different mechanical parts are coupled to perform nontrivial maneuvers. Similarly, our construction can also be applied to engineer acoustic or mechanical metamaterials with programmable response to external excitations[18,19].

Before we move on to present our results, we pause to comment on the boson-fermion correspondence discussed here. For non-interacting problems, both fermionic and bosonic Hamiltonians are characterized by a single-particle Hamiltonian $\mathcal{H}$, and the ground state (zero-temperature) behavior

of the system is determined by the 'filling' of the eigenmodes of $\mathcal{H}$. For fermions, Pauli exclusion dictates that all the eigenmodes up to the Fermi energy are filled in the zero-temperature limit. In particular, a 2D nodal semi-metal results if the Fermi surface consists entirely of nodal points, as in graphene (assuming spin-rotation invariance). The excitations about the ground state then correspond to quasi-particles with linear dispersion about some characteristic momentum $\boldsymbol{k}_c$.

Bosons in the zero-temperature limit, however, only occupy the lowest energy single-particle state(s) in the absence of interactions. Therefore, the stability of a free bosonic system requires $\mathcal{H}$ to be positive semi-definite. As such, one can write $\text{eig}(\mathcal{H}) = \{\omega^2\}$ with $\omega \geq 0$, and the ground state is gapped if and only if $\omega^2_{\text{min}} > 0$. A non-interacting 2D bosonic analogue of a semimetal will then be a system for which $\omega^2(\boldsymbol{k}_c) = 0$ at a collection of nodal points $\{\boldsymbol{k}_c\}$ (in the thermodynamic limit), since they would feature similar low-energy excitations. Strictly speaking, even the acoustic phonons satisfy the criterion outlined, but they are non-topological and can be trivially gapped out by breaking transition invariance (via, say, the introduction of a pinning potential). In contrast, here we are interested in the phonon analogue of *topological* nodal semimetals, where, in contrast to acoustic modes arising from conventional continuous symmetry breaking, the existence of the low-energy excitations are dictated by an underlying topological invariant.

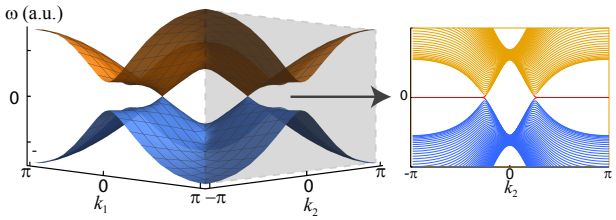

FIG. 1. Typical spectrum of a 2D TNS protected by chiral symmetry hosting a pair of topological nodes at $\omega = 0$ (only the two bands close to $\omega = 0$ are shown). The spectrum is computed for the fermionic problem defined in Eq. (2) with R defined in Eqs.(3) and (4). The parameters $(\theta_1, \phi_1, \theta_2, \phi_2) = (1/4, 0, 1/8, -1/8)\pi$ are used. The inset shows the edge spectrum when open and periodic boundary conditions are enforced for the $\hat{\boldsymbol{e}}_1$ and $\hat{\boldsymbol{e}}_2$ directions respectively, featuring a line of zero modes connecting the projections of the bulk topological nodes onto the surface Brillouin zone.

II. PHONON ANALOGUE OF TOPOLOGICAL NODAL SEMIMETALS

For a self-contained discussion, we first briefly describe phonon problems defined for mechanical structures formed by mass points connected by elastic elements modeled as central-force springs, and we review the boson-to-fermion mapping developed in Refs. [4–6]. The dynamics of such a system is determined by the kinetic energy of the mass points and the elastic potential energy stored in the springs, and therefore for N masses in d spatial dimension, a generic phonon problem can be defined by the Hamiltonian

$$H_B = \sum_{\boldsymbol{r}} \left(\frac{\boldsymbol{p}_{\boldsymbol{r}}^2}{2m_{\boldsymbol{r}}} + \frac{1}{2} \sum_{j=1}^{z/2} \kappa_{j,\boldsymbol{r}} s_{j,\boldsymbol{r}}^2 \right), \tag{1}$$

where $\boldsymbol{r}$ denotes the equilibrium positions of masses $m_{\boldsymbol{r}}$, $\boldsymbol{p}$ denotes momentum of the masses, z is the coordination number, and $s_{j,\boldsymbol{r}}$, $\kappa_{j,\boldsymbol{r}}$ are respectively the extension and spring constant of the j-th spring of the unit cell at $\boldsymbol{r}$. To simplify discussion, we set both $m_{\boldsymbol{r}}$ and $\kappa_{j,\boldsymbol{r}}$ to unity for all $(j, \boldsymbol{r})$ unless otherwise specified. Since we are interested in the existence of bulk zero modes, we also impose periodic boundary conditions.

The spring extensions $\{s_{j,\boldsymbol{r}}\}$ are functions of the displacements $\{\boldsymbol{x}_{\boldsymbol{r}}\}$ of the masses they connect. Within the harmonic approximation, the extensions are expanded to linear order in the mass displacements: $\boldsymbol{S} = R\boldsymbol{X} + \mathcal{O}(\boldsymbol{X}^2)$, where $\boldsymbol{X}$ is a dN dimensional column vector aggregating the displacement vectors of the N masses, and $\boldsymbol{S}$, similarly defined for the extensions $\{s_{j,\boldsymbol{r}}\}$, is $zN/2$ dimensional. The $zN/2 \times dN$ dimensional matrix R is physically a linear map relating the spring extensions to the mass displacements. R^T is known as the equilibrium matrix and it relates the acceleration of the masses to the spring extensions: $\ddot{\boldsymbol{X}} = -R^T\boldsymbol{S}$. As in[6], henceforth we restrict attention to isostatic lattices, which have $z = 2d$ and so R is a square matrix. With this notation, the phonon Hamiltonian, within the harmonic approximation, can be recast as $H_B = \frac{1}{2}\left[\boldsymbol{P}^2 + (R\boldsymbol{X})^2\right]$, where $\boldsymbol{P}$ is similarly defined as $\boldsymbol{X}$ and $R^TR = D$ is the real-space dynamical matrix. Equivalently, one can view R as a factorization of D.

The phonon modes are solutions to the eigenvalue problem $D\xi_i = R^TR\xi_i = \omega_i^2\xi$, where ω_i is the eigenfrequency of the i^{th} mode with $i = 1, \ldots, dN$. The bosonic phonon problem, characterized by R, can be mapped to a fermionic problem by considering a chiral matrix $\mathcal{H}_F$ and the associated Hamiltonian H_F[4–6]

$$\mathcal{H}_F = \begin{pmatrix} 0 & -iR^T \\ iR & 0 \end{pmatrix}; \; H_F = \begin{pmatrix} \bar{\boldsymbol{\chi}} & \boldsymbol{\chi} \end{pmatrix} \mathcal{H}_F \begin{pmatrix} \bar{\boldsymbol{\chi}} \\ \boldsymbol{\chi} \end{pmatrix}. \tag{2}$$

$\mathcal{H}_F$ satisfies $\{\tau^z, \mathcal{H}_F\} = 0$ with $\tau^z = \text{diag}(1_{dN\times dN}, -1_{dN\times dN})$. One can easily verify the $2dN$ eigenvalues of $\mathcal{H}_F$ are given by $\{\pm\omega_i\}$, which implies the phonon spectrum is encoded in the energy spectrum of the fermionic Hamiltonian H_F. We note that only a subset of the zero modes of $\mathcal{H}_F$ gives rise to zero modes of D; namely, those fermionic modes with $\tau^z = 1$. In contrast, fermionic zero-energy modes with $\tau^z = -1$ (i.e. null vectors of R^T) give rise to the so-called states of self-stress of the mechanical problem[6]. $\boldsymbol{\chi}, \bar{\boldsymbol{\chi}}$ are Majorana fermions satisfying $\{\chi_l, \chi_m\} = \{\bar{\chi}_l, \bar{\chi}_m\} = \delta_{lm}$ with all other anti-commutators vanishing. In particular, χ ($\bar{\chi}$) is even (odd) under time reversal (TR). Since H_F corresponds to a TR symmetric Hamiltonian of spinless fermions, it belongs to the Altland-Zirnbauer symmetry class BDI[20].

As the corresponding fermionic Hamiltonian is chiral, it can host topological nodes without fine-tuning even in 2D. To

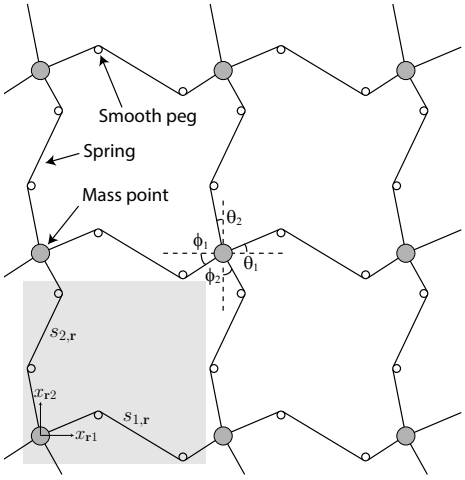

FIG. 2. A possible realization of the considered phonon problem. The dependence of the spring extensions on the displacements of the masses can be modified by bending the springs with fixed, smooth pegs which serve as a pinning potential and gap out the acoustic modes. The spring extensions are then characterized by Eq. (4) to linear order in mass displacements. The shaded region indicates the unit cell convention adopted.

find a phonon analogue inheriting the topological features of the TNS, therefore, we consider the phonon spectrum arising from a spring-mass model defined on the square lattice ($d = 2$ and $z = 4$). For a regular phonon problem, the form of R is constrained by global continuous translation invariance and spatial symmetries of the underlying lattice. For the square lattice, one simply finds $\omega_j(\boldsymbol{k}) \propto |\sin k_j|$, where $j = 1, 2$ labels the two orthogonal directions. Although $\omega_j(k_j = 0) = 0$, these nodal lines are not topologically protected as they can be gapped out by breaking translation symmetry.

Here we relax from these symmetry constraints and assume they are explicitly broken. A possible realization is depicted in Fig. 2, in which the springs are tweaked with fixed, smooth pegs that serve as an external pinning potential (a more realistic model is presented in Appendix A). The form of R, however, is still constrained by the geometrical relations between the spring extensions and mass displacements. For a spring connecting the masses at equilibrium positions $\boldsymbol{r} = \boldsymbol{a}$ and $\boldsymbol{b}$, the spring extension should satisfy $|s| \leq |\boldsymbol{x_a}| + |\boldsymbol{x_b}|$. In particular, we assume there is a special spatial direction $\boldsymbol{v} = \cos\theta_a \hat{\boldsymbol{e}}_1 + \sin\theta_a \hat{\boldsymbol{e}}_2$ such that the inequality is saturated for $\boldsymbol{x_a} = |\boldsymbol{x_a}|\boldsymbol{v}$ and $\boldsymbol{x_b} = \boldsymbol{0}$. Equivalently, this implies $\partial_{x_{\boldsymbol{a}1}} s = \cos\theta_a$ and $\partial_{x_{\boldsymbol{a}2}} s = \sin\theta_a$ in the original basis. Assuming a similar dependence of s on $\boldsymbol{x_b}$, characterized by $\boldsymbol{w} = \cos\theta_b \hat{\boldsymbol{e}}_1 + \sin\theta_b \hat{\boldsymbol{e}}_2$, one finds $s = \boldsymbol{v}\cdot\boldsymbol{x_a} + \boldsymbol{w}\cdot\boldsymbol{x_b} + \mathcal{O}(\boldsymbol{x}^2)$.

For a clean system, all springs that are equivalent under lattice translations are characterized by the same parameters and in momentum space one finds

$$R(\boldsymbol{k}) = \begin{pmatrix} v_{11} + w_{11}e^{-ik_1} & v_{12} + w_{12}e^{-ik_1} \\ v_{21} + w_{21}e^{-ik_2} & v_{22} + w_{22}e^{-ik_2} \end{pmatrix}, \quad (3)$$

where $\boldsymbol{k} = (k_1, k_2)$ lies in the first Brillouin zone (BZ), and v_{lm} (w_{lm}) denotes the m-th component of the vector $\boldsymbol{v}_l$ ($\boldsymbol{w}_l$), which relates the spring extension to the displacements $\boldsymbol{x_r}$ and $\boldsymbol{x}_{\boldsymbol{r}+\hat{\boldsymbol{e}}_l}$. Enforcing the geometric constraints, the vectors can be parameterized by

$$\begin{aligned} \boldsymbol{v}_1 &= \begin{pmatrix} -\cos\theta_1 \\ -\sin\theta_1 \end{pmatrix}; \boldsymbol{v}_2 = \begin{pmatrix} \sin\theta_2 \\ -\cos\theta_2 \end{pmatrix}; \\ \boldsymbol{w}_1 &= \begin{pmatrix} \cos\phi_1 \\ \sin\phi_1 \end{pmatrix}; \boldsymbol{w}_2 = \begin{pmatrix} -\sin\phi_2 \\ \cos\phi_2 \end{pmatrix}. \end{aligned} \quad (4)$$

The sign convention of the angles are chosen to match the parameterization in Fig. 2. The corresponding fermionic Hamiltonian, as defined in Eq. (2), is explicitly given by

$$H_F = 2i \sum_{\boldsymbol{r}} \sum_{l,m=1}^{2} \left(v_{lm} \chi^l_{\boldsymbol{r}} \bar{\chi}^m_{\boldsymbol{r}} + w_{lm} \chi^l_{\boldsymbol{r}} \bar{\chi}^m_{\boldsymbol{r}+\hat{\boldsymbol{e}}_l} \right). \quad (5)$$

Although the BDI class is topologically trivial in 2D, the system can inherit the nontrivial properties of the 1D system when identical 1D chains are stacked in one direction, similar to weak topological insulators. To this end, we introduce Fourier-transformed variables

$$\chi^l_{\boldsymbol{r}} = \frac{1}{\sqrt{N_2}} \sum_{k_2} \chi^l_{x_1,k_2} e^{-ik_2 x_2}; \ \chi^l_{x_1,k_2} = \frac{1}{\sqrt{N_2}} \sum_{x_2} \chi^l_{\boldsymbol{r}} e^{ik_2 x_2}, \quad (6)$$

where N_j is the number of sites along the $\hat{\boldsymbol{e}}_j$ direction, and $\bar{\chi}^l_{x_1,k_2}$ is similarly defined. Since $(\chi^l_{x_1,k_2})^\dagger = \chi^l_{x_1,-k_2}$ is complex, one can define Majorana operators for $k_2 \in (0, \pi)$

$$\lambda_{x_1,|k_2|} = \frac{\chi^l_{x_1,k_2} + \chi^l_{x_1,-k_2}}{2}; \ \eta_{x_1,|k_2|} = \frac{\chi^l_{x_1,k_2} - \chi^l_{x_1,-k_2}}{2i}, \quad (7)$$

which are both even under TR. $\bar{\lambda}_{x_1,|k_2|}$ and $\bar{\eta}_{x_1,|k_2|}$, similarly defined for $\bar{\chi}_{x_1,k_2}$, are odd under TR. Since Eq.(5) only couples χ to $\bar{\chi}$, upon Fourier transform $H_F(k_2)$ will only couple (λ, η) to $(\bar{\lambda}, \bar{\eta})$ and each such 1D system is in the BDI class. While the BDI class is classified by $\mathbb{Z}$ in 1D, the indexes of the 1D chains here are always even: the original lattice translational symmetry along $\hat{\boldsymbol{x}}_2$, reflected as a local $\mathcal{O}(2)$ rotation between $(\lambda_{x_1,|k_2|}, \eta_{x_1,|k_2|})$, guarantees that the Majorana zero modes at each edge occur in pairs. This can also be understood from the doubling of Majorana modes for each $k_2 \in (0, \pi)$, as $\chi^l_{x_1,k_2}$ and $\chi^l_{x_1,-k_2}$ are now Hermitian conjugates of each other. Such property of the system is more manifest by relabeling the operators as

$$c^A_{l,x,k_2} \equiv \chi^l_{x_1,k_2}; \ \ c^B_{l,x,k_2} \equiv \bar{\chi}^l_{x_1,k_2}; \ k_2 \in (0, \pi) \quad (8)$$

such that c_l's are complex fermions. Eq.(5) is then decoupled into a series of 1D fermionic Hamiltonians, each labeled by $k_2 \in (0, \pi)$,

$$\begin{aligned} H_F(k_2) = 2 \sum_x \Big[& i v_{11} c^{A\dagger}_{1,x} c^B_{1,x} + i v_{12} c^{A\dagger}_{1,x} c^B_{2,x} \\ & + i w_{11} c^{A\dagger}_{1,x} c^B_{1,x+1} + i w_{12} c^{A\dagger}_{1,x} c^B_{2,x+1} \\ & + i(v_{21} + w_{21} e^{-ik_2}) c^{A\dagger}_{2,x} c^B_{1,x} \\ & + i(v_{22} + w_{22} e^{-ik_2}) c^{A\dagger}_{2,x} c^B_{2,x} + h.c. \Big], \end{aligned} \quad (9)$$

where we have suppressed the subscript k_2 on the operators. The original chiral symmetry is manifested in this notation as a sublattice (A-B) symmetry.

To characterize these 1D systems, we further Fourier transform on x, which gives

$$H_F(k_2) = 2\sum_{k_1} \begin{pmatrix} \boldsymbol{c}^{A\dagger} & \boldsymbol{c}^{B\dagger} \end{pmatrix} \begin{pmatrix} 0 & iR_{\boldsymbol{k}} \\ -iR_{\boldsymbol{k}}^\dagger & 0 \end{pmatrix} \begin{pmatrix} \boldsymbol{c}^A \\ \boldsymbol{c}^B \end{pmatrix}, \tag{10}$$

where the subscript $\boldsymbol{k}$ of the operators is suppressed, $\boldsymbol{c}^A = (c_1^A, c_2^A)^T$, and similarly for $\boldsymbol{c}^B$. The bulk topological invariant of $\mathcal{H}_F(k_2)$ is given by the winding number of $\det(iR_{\boldsymbol{k}})$ as k_1 is varied from $-\pi$ to π[7]. More explicitly, we have

$$\begin{aligned} \det(iR_{\boldsymbol{k}}) =& -\left([\boldsymbol{v}_1 \wedge \boldsymbol{v}_2] + [\boldsymbol{v}_1 \wedge \boldsymbol{w}_2]e^{-ik_2}\right) \\ & -\left([\boldsymbol{w}_1 \wedge \boldsymbol{v}_2] + [\boldsymbol{w}_1 \wedge \boldsymbol{w}_2]e^{-ik_2}\right)e^{-ik_1} \\ \equiv& r_1(k_2) + r_2(k_2)e^{-ik_1}, \end{aligned} \tag{11}$$

where $[\boldsymbol{v} \wedge \boldsymbol{w}]$ denotes the component of the wedge product $\boldsymbol{v} \wedge \boldsymbol{w}$ in the $\hat{\boldsymbol{e}}_1 \wedge \hat{\boldsymbol{e}}_2$ direction, and $r_1(k_2)$, $r_2(k_2)$ are introduced to simplify the expressions. The winding number $\mathcal{W}_{k_2}$ is determined by the relative magnitude of $|r_1(k_2)|$ and $|r_2(k_2)|$. The case of particular interest is when the winding numbers $\mathcal{W}_{k_2\to 0^+} \neq \mathcal{W}_{k_2\to\pi^-}$, which implies there must be a topological phase transition as k_2 is changed from 0 to π. Such a phase transition occurs when

$$\frac{|r_1(0)r_1(\pi)| + |r_2(0)r_2(\pi)|}{|r_1(0)r_2(\pi)| + |r_2(0)r_1(\pi)|} < 1, \tag{12}$$

and when this is satisfied the gap at $E = 0$ must close at some critical quasi-momentum $\boldsymbol{k}_c$, giving rise to a topological node. Such nodes in the fermionic picture are reflected in the original bosonic problem as a pair of isolated points $\pm\boldsymbol{k}_c$ at which the phonon frequency vanishes, corresponding to a bulk zero mode in the linearized spectrum.

For a system parameterized as in Eq. (4), we have

$$\begin{aligned} &\frac{|r_1(0)r_1(\pi)| + |r_2(0)r_2(\pi)|}{|r_1(0)r_2(\pi)| + |r_2(0)r_1(\pi)|} \\ =& \max\{|\cos(\theta_1 - \phi_1)|, |\cos(\theta_1 + \phi_1 - \theta_2 - \phi_2)|\}, \end{aligned} \tag{13}$$

which implies that, for general parameters, its linearized phonon spectrum always contains a topologically protected bulk zero mode. Note that if $\theta_1 + \phi_1 - \theta_2 - \phi_2$ is an integer multiple of π then ω accidentally vanishes on a pair of arcs in the BZ, rendering $\mathcal{H}_F(|k_2|)$ gapless for all $|k_2|$. For generic parameters, the critical quasi-momentum is

$$\boldsymbol{k}_c = (\theta_1 - \phi_1)\hat{\boldsymbol{x}} + (\theta_2 - \phi_2)\hat{\boldsymbol{y}}, \tag{14}$$

and therefore the quasi-momentum associated with the protected bulk zero mode can be adjusted simply by tuning the angles θ_j and ϕ_j.

III. DISPERSION AND ROBUSTNESS OF ZERO MODES

A. Conical phonon dispersion for the smooth peg model

For a stable system, the phonon frequencies satisfy $\omega_\pm^2(\boldsymbol{k}) \geq 0$, where the $\pm$ sign corresponds to the two branches from diagonalizing the 2×2 dynamical matrix $D_{\boldsymbol{k}}$. As such $\omega_-^2(\boldsymbol{k})$ attains a global minimum at $\boldsymbol{k}_c$ and therefore $\boldsymbol{\nabla}_{\boldsymbol{k}}\omega_0|_{\boldsymbol{k}_c} = \boldsymbol{0}$. Expanding $\omega_-^2(\boldsymbol{k})$ around the nodal point $\boldsymbol{k}_c$, we have

$$\omega_-^2(\boldsymbol{k}_c + \delta\boldsymbol{k}) \approx \frac{1}{2}\sum_{ij} \frac{\partial^2(\omega_-^2)}{\partial k_i \partial k_j}\bigg|_{\boldsymbol{k}_c} \delta k_i \delta k_j. \tag{15}$$

The phonon speeds around the conical dispersion is given by:

$$\frac{1}{2}\left(\frac{\partial^2(\omega_-^2)}{\partial k_i \partial k_j}\right)\bigg|_{\boldsymbol{k}_c} = \frac{\kappa_1\kappa_2}{2(\kappa_1\mathcal{S}_1^2 + \kappa_2\mathcal{S}_2^2)} \begin{pmatrix} \mathcal{S}_2^2 & \mathcal{S}_1\mathcal{S}_2\mathcal{C}_\delta \\ \mathcal{S}_1\mathcal{S}_2\mathcal{C}_\delta & \mathcal{S}_1^2 \end{pmatrix} \tag{16}$$

where we let $\mathcal{S}_j = \sin k_{cj}$ with $k_{cj} = \theta_j - \phi_j$ for $j = 1, 2$, and $\mathcal{S}_\delta = \sin\delta$, $\mathcal{C}_\delta = \cos\delta$ with $\delta = \theta_1 + \phi_1 - \theta_2 - \phi_2$. The characteristic speeds around the nodal point is therefore given by

$$c_\pm^2 = \frac{\kappa_1\kappa_2(\mathcal{S}_1^2 + \mathcal{S}_2^2)}{4(\kappa_1\mathcal{S}_1^2 + \kappa_2\mathcal{S}_2^2)} \left(1 \pm \sqrt{1 - \left(\frac{2\mathcal{S}_1\mathcal{S}_2\mathcal{S}_\delta}{\mathcal{S}_1^2 + \mathcal{S}_2^2}\right)^2}\right). \tag{17}$$

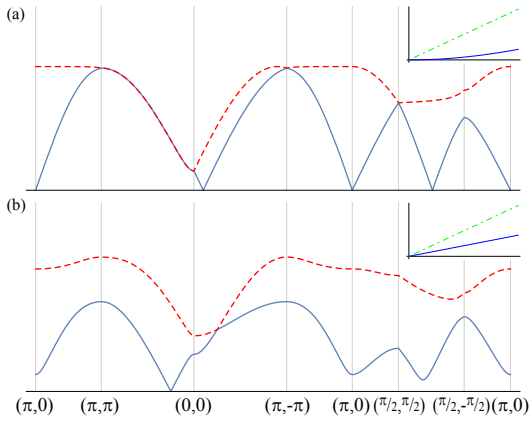

FIG. 3. Linearized phonon spectrum for the smooth peg model along different paths in the 2D BZ. The insets show the dispersion of the two independent phonon modes around the critical quasi-momentum $\boldsymbol{k}_c$. As in the text here we take $m = \kappa_1 = \kappa_2 = 1$. (a) The parameters $(\theta_1, \phi_1, \theta_2, \phi_2) = (0.1, 0.2, 0.2, 0.1)\pi$ are used. As such $\theta_1 + \phi_1 - \theta_2 - \phi_2 = 0$, which gives rise to an accidental vanishing of ω along a pair of arcs in BZ. This is seen in the vanishing of ω at multiple values of $\boldsymbol{k}$ as well as the existence of a quadratic phonon mode around $\boldsymbol{k}_c$. (b) The parameters $(\theta_1, \phi_1, \theta_2, \phi_2) = (1/4, 0, 1/8, -1/8)\pi$ are used (same as Fig. 1 of the main text), which corresponds to the generic case in which the linearized phonon spectrum contains a pair of isolated bulk nodal points at $\pm\boldsymbol{k}_c$ with conical dispersion around them.

It is clear that when $\delta = 0$, we have $c_- = 0$, corresponding to the softening of the phonon mode due to the line node; when $\delta = \pi/2$ and $\mathcal{S}_1^2 = \mathcal{S}_2^2$, we have $c_+ = c_-$ and this gives an isotropic conical dispersion.

B. Robustness

Since the two topological nodes located at $\pm\boldsymbol{k}_c \neq \mathbf{0}$ are isolated in momentum space, they are robust, in the fermionic picture, against small perturbations respecting chiral symmetry. This implies the phonon analogue is robust against weak arbitrary perturbations to the rigidity matrix R, accommodating all the natural perturbations in a spring-mass model. Such robustness is demonstrated in the finite-size scaling shown in Fig. 4, in which we evaluate the disorder average of the lowest eigenfrequency found by numerically diagonalizing the linearized dynamical matrix. The sharp dips at $N = 40^2$ and 80^2 originate from the commensuration between the finite momentum mesh and $\boldsymbol{k}_c = \pm(1/4, 1/4)\pi$. In the presence of disorder ($\sigma \neq 0$) the quasi-momentum ceases to be a good quantum number, but the bulk zero mode remains, as demonstrated by the decrease of $\langle\omega^2_{min}\rangle$ as system size increases.

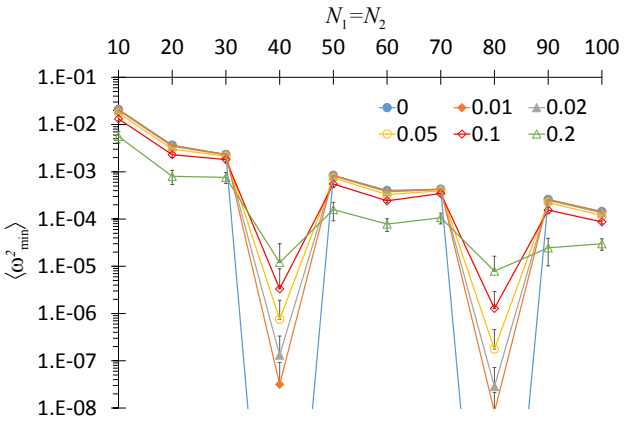

FIG. 4. Finite size scaling of the lowest eigenvalue of the disordered dynamical matrix. The linearized dynamical matrix for systems with size $N = N_1 N_2$ and site-dependent couplings is numerically diagonalized to find the smallest eigenvalue ω^2_{min}. The clean system is defined by the same set of parameters used in Fig. 1. Disorder is incorporated by adding to each parameter at each site a small, independent deviation drawn from a normal distribution with standard deviation σ (κ and m are kept non-negative by taking absolute values). For each σ, the mean value $\langle\omega^2_{\text{min}}\rangle$ is obtained from 200 disorder realizations. Error bars represent standard deviation in the disorder averages, and solid lines are guides for the eye.

In the presence of disorder, however, one can reasonably question whether the zero mode observed is really an extended bulk modes, or corresponds to local "rattlers". In Fig. 5 we plot the disorder average of the variance of the center-of-mass for the state found. The various curves with different disorder strengths collapse to the disorder-free one, indicating the mode remains extended in nature for the disorder strengths considered.

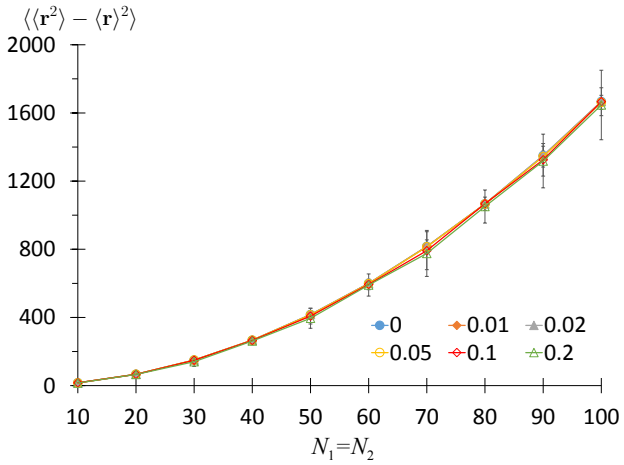

FIG. 5. Disorder average of the spatial profile of the lowest-frequency mode. Error bars indicate standard deviation from the disorder averaging.

Since the extended soft modes demonstrated here are protected by the topological properties of the linearized problem, one expects these modes to be only infinitesimal instead of finite. In addition, when the spring-mass description is only a model for a more general system, natural perturbations like the inclusion of small further neighbor couplings correspond to perturbations to the dynamical matrix instead of the rigidity matrix. Such perturbations can render the problem at hand non-isostatic and completely alter the structure of the analysis. The topological protection of the modes is generally lost when confronted with such perturbations. Therefore, we distinguish between the usefulness of this mapping when the bosonic problem is interpreted in a mechanical context (as done here), where local isostaticity is a binary question, as opposed to a quantum mechanical problem obtained after quantization, for which local isostaticity may only be an approximation[21].

IV. CONCLUSIONS

In summary, we show that the mapping of bosonic phonon problems to chiral fermionic problems can be used to construct phonon analogues of topological nodal semimetals. In particular, we construct a 2D system that hosts a tunable bulk extended mode in its linearized phonon spectrum even when global translation symmetry is broken by an external pinning potential. Contrary to usual collective phonon modes arising from continuous symmetry breaking, the existence of such modes is not dictated by symmetry and has its roots in the topological properties of the corresponding fermionic problem. We also emphasize that the topological modes we discussed in this work, which we often refer to as the 'topological zero-modes', are readily excited at a vanishing probe frequency. In practice, these modes acquire a small excitation gap limited by the finite system size (corresponding to an imperfect sampling of the BZ in the clean limit) and the applicability of the harmonic approximation. This is in stark contrast

to the previously discussed topological bosonic modes in, for instance, Refs.[15–17], which correspond to finite-frequency excitations of the system.

Such gapless topological bosonic modes are robust against disorder within the linearized description. Such modes should be contrasted with the conventional acoustic modes, which have a completely different origin and are non-topological in nature. It is also worthwhile to point out that disordered, globally isostatic mechanical frames can nonetheless contain over- and under-coordinated regions, and the under-coordinated regions will in general feature localized, 'rattling' zero modes. In contrast, the topological modes discussed in this work remain extended even when disorder is introduced. These topological modes, however, are expected to be gapped when one performs a full phonon spectrum analysis incorporating anharmonicity. As long as the harmonic approximation is justified, the real phonon spectrum still contains such bulk soft modes at finite wavevector and they can be utilized to engineer metamaterials and mechanical structures with fault-tolerant properties.

In finalizing this manuscript, we became aware of a complimentary investigation[22] by Rocklin *et al.* addressing the same problem from a different perspective.

Acknowledgment - We thank Haruki Watanabe and Anton Akhmerov for discussions. AV was supported by ARO MURI Grant W 911-12-0461. HCP appreciates financial support from the Hellman Fellows Fund; YB acknowledges funding from NSF GRFP under Grant No. DGE 1106400.

Appendix A: An alternative model

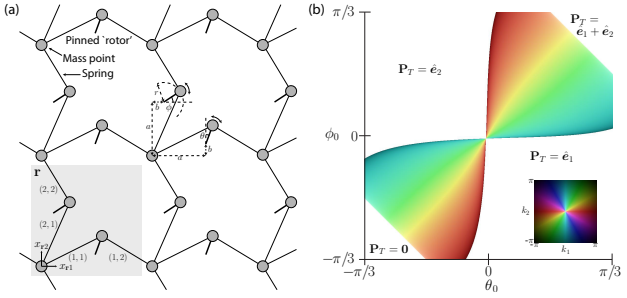

FIG. 6. An alternative model in which the smooth pegs are replaced by pinned rotors, which preserves isostaticity. (a) Schematic of the model indicating the different parameters. The shaded region indicates the choice of the unit cell, and each spring in the cell is labeled by a pair of numbers (l, m). (b) Example phase diagram with $a = 0.4$, $b = -0.15$, $r = 0.1$ and $\theta_0,\ \phi_0 \in [-\pi/3, \pi/3]$. The colored region corresponds to the TNS phase, with the color (inset) encoding the value of $\pm\boldsymbol{k}_c$. The white regions correspond to a gapped phonon spectrum, which can still have different topological polarization $\boldsymbol{P}_T$.

Here we provide an alternative model that is both more realistic and also exhibits a richer phase diagram. Instead of connecting adjacent mass points by springs sliding over smooth pegs, we considering connecting them via pinned, rigid rotors similar to those discussed in Ref.[6] (Fig. 6a). By 'rotor' we refer to a mass point restricted to rotate on a circle by a rigid rod of negligible mass. This introduces two extra degrees of freedom in each unit cell, but at the same time each of the original spring is replaced by two springs. Altogether the balance between number of degrees of freedom and constraints is maintained, i.e. isostaticity is preserved.

Each rotor introduced can be characterized by four parameters: mass m, radius r of the circle it sweeps out, and the coordinate (a, b) of the pinning point relative to the origin of the unit cell. While these parameters can be different for the two rotors in the unit cell, for simplicity we characterize them by the same set of parameter (m, r, a, b) (see Fig. 6a). In particular, we set the mass m to be the same as that of the mass points. The spring constants for all springs are also set to the same value κ. We set the lattice constant to 1. As such, there are still two system parameters: θ_0 and ϕ_0, which characterize the tilt of the rotors with respect to the coordinate axes at equilibrium. The equilibrium lengths of the springs (assuming no pre-stress), ℓ_{lm}, can then be written in terms of these parameters:

$$\begin{aligned}\ell_{11} =& \sqrt{(b + r\cos\theta_0)^2 + (a + r\sin\theta_0)^2};\\ \ell_{12} =& \sqrt{(b + r\cos\theta_0)^2 + (1 - a - r\sin\theta_0)^2};\end{aligned} \tag{A1}$$

and ℓ_{21}, ℓ_{22} take the same form as ℓ_{11}, ℓ_{12} but with $\theta_0 \to \phi_0$.

The energy of the system is

$$\begin{aligned}E =& \frac{m}{2}\sum_{\boldsymbol{r}}\left(\dot{x}^2_{\boldsymbol{r}1} + \dot{x}^2_{\boldsymbol{r}2} + r^2(\dot{\theta}^2_{\boldsymbol{r}} + \dot{\phi}^2_{\boldsymbol{r}})\right)\\ &+ \frac{\kappa}{2}\sum_{\boldsymbol{r}}\sum_{l,m=1}^{2} s^2_{lm,\boldsymbol{r}},\end{aligned} \tag{A2}$$

where $x_{l\boldsymbol{r}}$ denotes the displacement in the $\hat{\boldsymbol{e}}_l$ direction for the mass point in the unit-cell labeled by $\boldsymbol{r}$, and $s_{lm,\boldsymbol{r}}$ denotes the spring extension of the (l, m)-th spring in the unit cell, as indicated in Fig. 6a. As in the main text, we linearize $s_{lm,\boldsymbol{r}}$ and obtain the rigidity matrix via $\boldsymbol{S} = R\boldsymbol{X} + \mathcal{O}(\boldsymbol{X}^2)$, where $\boldsymbol{X}$ is the collective vector for the small fluctuations $\{x_{\boldsymbol{r}1}, x_{\boldsymbol{r}2}, r\delta\theta_{\boldsymbol{r}}, r\delta\phi_{\boldsymbol{r}}\}$ with $\delta\theta_{\boldsymbol{r}} = \theta_{\boldsymbol{r}} - \theta_0$ and $\delta\phi_{\boldsymbol{r}} = \phi_{\boldsymbol{r}} - \theta_0$. After Fourier transform, one finds

$$R_{\boldsymbol{k}} = \ell^{-1} \begin{pmatrix} -a - r\sin\theta_0 & -b - r\cos\theta_0 & a\cos\theta_0 - b\sin\theta_0 & 0 \\ (1-a-r\sin\theta_0)e^{-ik_1} & -(b + r\cos\theta_0)e^{-ik_1} & -(1-a)\cos\theta_0 - b\sin\theta_0 & 0 \\ -b - r\cos\phi_0 & -a - r\sin\phi_0 & 0 & a\cos\phi_0 - b\sin\phi_0 \\ -(b + r\cos\phi_0)e^{-ik_2} & (1-a-r\sin\phi_0)e^{-ik_2} & 0 & -(1-a)\cos\phi_0 - b\sin\phi_0 \end{pmatrix}, \tag{A3}$$

where $\ell = \mathrm{diag}(\ell_{11}, \ell_{12}, \ell_{21}, \ell_{22})$.

As in the main text, the phase of the system is encoded in the winding numbers of the corresponding fermionic Hamiltonians $\mathcal{H}_F(k_2)$, which we write as

$$\begin{aligned} \det\left(iR_{\boldsymbol{k}}\right) =& \left(\tilde{v}_1 + \tilde{v}_2\, e^{-ik_2}\right) + \left(\tilde{w}_1 + \tilde{w}_2\, e^{-ik_2}\right) e^{-ik_1} \\ \equiv& \tilde{r}_1(k_2) + \tilde{r}_2(k_2)\, e^{-ik_1}. \end{aligned} \tag{A4}$$

The winding number $\mathcal{W}_{k_2}$ is determined by $|\tilde{r}_1(k_2)|/|\tilde{r}_2(k_2)|$. After some algebra, one sees that it is determined by the sign of

$$\begin{aligned} \tilde{f}(k_2) =& (\tilde{v}_1^2 + \tilde{v}_2^2 - \tilde{w}_1^2 - \tilde{w}_2^2) + 2(\tilde{v}_1\tilde{v}_2 - \tilde{w}_1\tilde{w}_2)\cos(k_2) \\ \equiv& \tilde{f}_1 + \tilde{f}_2\cos(k_2), \end{aligned} \tag{A5}$$

where $\tilde{f}_1$ and $\tilde{f}_2$ are both real. More concretely, $\mathcal{W}_{k_2} = 0\ \forall k_2$ if $\tilde{f}_1 > |\tilde{f}_2|$; $\mathcal{W}_{k_2} = -1\ \forall k_2$ if $\tilde{f}_1 < -|\tilde{f}_2|$; and $\mathcal{W}_{k_2\to 0+} \neq \mathcal{W}_{k_2\to\pi^-}$ otherwise, indicating the system is in the TNS phase. For the first two cases, $\mathcal{W}_{k_2}$ is independent of k_2 and it is meaningful to define the integer $n_1 = -\mathcal{W}_{k_2}$.

The same analysis can be performed with the role of k_1 and k_2 interchanged, giving the winding number $\mathcal{W}_{k_1}$. When the phonon spectrum is gapped, the topological polarization $\boldsymbol{P}_T = n_1\hat{\boldsymbol{e}}_1 + n_2\hat{\boldsymbol{e}}_2$ is well defined[6,12]. We plot in Fig. 6b an example phase diagram of the system, demonstrating all the mentioned phases with different topological polarizations can be accessed in this model.

[1] S. Sachdev, *Quantum Phase Transitions*, Troisième Cycle de la Physique (Cambridge University Press, 2011), ISBN 9781139500210.
[2] X.-G. Wen, *Quantum field theory of many-body systems* (Oxford University Press, 2004).
[3] J. van Hemmen, Zeitschrift für Physik B Condensed Matter **38**, 271 (1980), ISSN 0722-3277.
[4] V. Gurarie and J. T. Chalker, Phys. Rev. Lett. **89**, 136801 (2002).
[5] V. Gurarie and J. T. Chalker, Phys. Rev. B **68**, 134207 (2003).
[6] C. L. Kane and T. C. Lubensky, Nat Phys **10**, 39 (2014), ISSN 1745-2473.
[7] M. Franz and L. Molenkamp, eds., *Topological Insulators*, vol. 6 of *Contemporary Concepts of Condensed Matter Science* (Elsevier, 2013).
[8] X. Wan, A. M. Turner, A. Vishwanath, and S. Y. Savrasov, Phys. Rev. B **83**, 205101 (2011).
[9] A. A. Burkov, M. D. Hook, and L. Balents, Phys. Rev. B **84**, 235126 (2011).
[10] V. Vitelli, N. Upadhyaya, and B. Gin-ge Chen, ArXiv e-prints (2014), 1407.2890.
[11] B. Gin-ge Chen, N. Upadhyaya, and V. Vitelli, ArXiv e-prints (2014), 1404.2263.
[12] J. Paulose, B. Gin-ge Chen, and V. Vitelli, ArXiv e-prints (2014), 1406.3323.
[13] K. Sun, A. Souslov, X. Mao, and T. C. Lubensky, Proceedings of the National Academy of Sciences **109**, 12369 (2012).
[14] O. Vafek and A. Vishwanath, Annual Review of Condensed Matter Physics **5**, 83 (2014).
[15] L. Lu, L. Fu, J. D. Joannopoulos, and M. Soljačić, Nature Photonics **7**, 294 (2013).
[16] M. Xiao, W.-J. Chen, W.-Y. He, and C. T. Chan, Nature Physics **11**, 920 (2015).
[17] Y.-T. Wang, P.-G. Luan, and S. Zhang, New Journal of Physics **17**, 073031 (2015), URL http://stacks.iop.org/1367-2630/17/i=7/a=073031.
[18] R. Craster and S. Guenneau, *Acoustic Metamaterials: Negative Refraction, Imaging, Lensing and Cloaking*, Springer Series in Materials Science (Springer, 2012), ISBN 9789400748132.
[19] B. Florijn, C. Coulais, and M. van Hecke, ArXiv e-prints (2014), 1407.4273.
[20] A. Altland and M. R. Zirnbauer, Phys. Rev. B **55**, 1142 (1997).
[21] M. J. Lawler, ArXiv e-prints (2015), 1510.03697.
[22] D. Zeb Rocklin, B. Gin-ge Chen, M. Falk, V. Vitelli, and T. C. Lubensky, ArXiv e-prints (2015), 1510.04970.